SIGNAL RECOVERY FROM PARTIAL FRACTIONAL FOURIER DOMAIN INFORMATION AND PULSE SHAPE DESIGN USING ITERATIVE PROJECTIONS

A THESIS

SUBMITTED TO THE DEPARTMENT OF ELECTRICAL AND

ELECTRONICS ENGINEERING

AND THE INSTITUTE OF ENGINEERING AND SCIENCE

OF BILKENT UNIVERSITY

IN PARTIAL FULFILLMENT OF THE REQUIREMENTS

FOR THE DEGREE OF

MASTER OF SCIENCE

By

H. Emre Güven

July, 2005

I certify that I have read this thesis and that in my opinion it is fully adequate, in scope and in quality, as a thesis for the degree of Master of Science.

Prof. Dr. A. Enis Çetin (Co-Supervisor)

I certify that I have read this thesis and that in my opinion it is fully adequate, in scope and in quality, as a thesis for the degree of Master of Science.

Prof. Dr. Haldun M. Özaktaş (Co-Supervisor)

I certify that I have read this thesis and that in my opinion it is fully adequate, in scope and in quality, as a thesis for the degree of Master of Science.

Asst. Prof. Dr. Defne Aktaş

I certify that I have read this thesis and that in my opinion it is fully adequate, in scope and in quality, as a thesis for the degree of Master of Science.

Dr. Çağatay Candan

Approved for the Institute of Engineering and Science:

Prof. Dr. Mehmet Baray
Director of the Institute of Engineering and Science

ABSTRACT

SIGNAL RECOVERY FROM PARTIAL FRACTIONAL FOURIER DOMAIN INFORMATION AND PULSE SHAPE DESIGN USING ITERATIVE PROJECTIONS

H. Emre Güven
M.S. in Electrical and Electronics Engineering
Supervisors: Prof. Dr. A. Enis Çetin and
Prof. Dr. Haldun M. Özaktaş
July, 2005

Signal design and recovery problems come up in a wide variety of applications in signal processing. In this thesis, we first investigate the problem of pulse shape design for use in communication settings with matched filtering where the rate of communication, intersymbol interference, and bandwidth of the signal constitute conflicting themes. In order to design pulse shapes that satisfy certain criteria such as bit rate, spectral characteristics, and worst case degradation due to intersymbol interference, we benefit from the wellknown Projections Onto Convex Sets. Secondly, we investigate the problem of signal recovery from partial information in fractional Fourier domains. Fractional Fourier transform is a mathematical generalization of the ordinary Fourier transform, the latter being a special case of the first. Here, we assume that low resolution or partial information in different fractional Fourier transform domains is available in different intervals. These information intervals define convex sets and can be combined within the Projections Onto Convex Sets framework. We present generic scenarios and simulation examples in order to illustrate the use of the method.

Keywords: Projections onto convex sets, fractional Fourier transform, iterative signal design, iterative signal recovery.

ÖZET

ÖZYİNELİ İZDÜŞÜMLER KULLANARAK KISMİ KESİRLİ FOURIER DÖNÜŞÜMÜ BİLGİSİNDEN İŞARET GERİ KAZANIMI VE DARBE ŞEKLİ TASARIMI

H. Emre Güven
Elektrik ve Elektronik Mühendisliği, Yüksek Lisans
Tez Yöneticileri: Prof. Dr. A. Enis Çetin ve
Prof. Dr. Haldun M. Özaktaş
Temmuz, 2005

İşaret tasarım ve geri kazanım problemleri işaret işleme uygulamalarında sık olarak karşımıza çıkmaktadır. Bu tezde ilk olarak, uyumlu filtre kullanılan bir iletişim sisteminde bant genişliği, iletişim oranı ve semboller arası girişim gibi çelişen temalar arasında belirli ölçütleri sağlayan bir darbe şekli tasarlama problemini inceliyoruz. Bit oranı, spektral dağılım ve semboller arası girişimden dolayı en kötü durum başarımı gibi kriterleri sağlayan bir çözüm bulmak için dışbükey kümeler üzerine izdüşümler yöntemini kullanıyoruz. Tezin ikinci bölümünde ise, kesirli Fourier uzaylarında kısmi bilgilerden işaret geri kazanımı problemini inceliyoruz. Kesirli Fourier dönüşümü, iyi bilinen Fourier dönüşümünün matematiksel genelleştirilmesidir. Burada, kesirli Fourier uzaylarında düşük çözünürlükte veya farklı aralıklarda kısmi bilgilerin var olduğunu varsayıyoruz. Bu bilgi aralıkları dışbükey kümeler tanımlar ve Dışbükey Kümeler Üzerine İzdüşüm çerçevesinde birleştirilebilir. Yöntemin kullanımını göstermek için genel senaryolar ve benzetim örnekleri sunuyoruz.

Anahtar sözcükler: Dışbükey kümeler üzerine izdüşüm, kesirli Fourier dönüşümü, özyineli işaret tasarımı, özyineli işaret geri kazanımı.

Acknowledgement

Firstly, I would like to express my thanks and gratitude to my supervisors Prof. Dr. A. Enis Çetin and Prof. Dr. Haldun M. Özaktaş for their enlightening guidance and unlimited support in the supervision of the thesis.

Secondly, I would like to express my thanks to Asst. Prof. Dr. Defne Aktaş, Assoc. Prof. Dr. Orhan Arıkan, and Dr. Çağatay Candan for showing keen interest and accepting to read and review the thesis. I would also like to thank Asst. Prof. Dr. Defne Aktaş for her inspirational introduction to the pulse shape design problem.

Furthermore, I would like to thank my manager Ufuk Kazak at Aselsan Inc. for encouraging me to continue with my studies. Special thanks to my friend and colleague Aykut Arıkan for many hours of fruitful technical discussions.

Finally, I thank my beloved wife Handan with deepest appreciation for her incessant encouragement and motivation.

Contents

List of Figures

Chapter 1

Introduction

Signal design and recovery problems come up in a wide variety of applications in signal processing. Among the myriad of mathematical tools used developed for these problems, the technique of projections onto convex sets (POCS) [1–3, 5–10, 48] is of special interest due to its success in incorporating knowledge that can be tedious to work with using analytical methods. POCS presents a straightforward approach in finding a solution to a given problem, by imposing several constraints on consecutive iterations. Furthermore, another desired property of POCS is its guaranteed convergence, regardless of the initial point of iterations. In this thesis, we use the method of POCS in two different problems.

First, we investigate problem of pulse shape design for use in communication settings with matched filtering where the rate of communication, intersymbol interference (ISI), and bandwidth of the signal constitute conflicting themes [44]. In order to design pulse shapes that satisfy certain criteria such as bit rate, spectral characteristics, and worst case degradation due to intersymbol interference, we benefit from the method of POCS. We design several exemplary pulse shapes that satisfy certain constraints such as spectral masks and bounds on worst case degradation due to ISI, through iterative methods.

Next, we investigate the problem of signal recovery from partial information in

fractional Fourier domains. Fractional Fourier transform (FRT) [11–39] is a mathematical generalization of the ordinary Fourier transform, the latter being a special case of the first. It has found many applications in optics and signal processing, adding an order dimension to the concept of spectral analysis. Here, we assume that low resolution or partial information in different fractional Fourier transform domains is available in differend bands. These information bands define convex sets and can be combined within a POCS framework. We present generic application scenarios and simulation examples in order to illustrate the use of the method.

The outline of the thesis is as follows: In Chapter 2, we introduce some background on the method of Projections Onto Convex Sets and fractional Fourier transform. Chapter 3 presents the pulse shape design problem and several examples illustrating the use of iterative design method. We expose the signal recovery problem in Chapter 4 along with several application scenarios and simulation examples. Finally, we present the conclusions of the thesis and future work in Chapter 5.

Chapter 2

Background

2.1 Projections Onto Convex Sets

In this section we present a background on the method of projections onto convex sets (POCS) [1–3] that has been successfully used in many signal recovery and restoration problems [4–10]. The key idea is to obtain a solution which is consistent with all the available information. In this method the set of all possible signals is assumed to constitute a Hilbert space with an associated norm in which the prior information about the desired signal can be represented in terms of convex sets. In this thesis, the Hilbert space is L^2 or ℓ^2 with Euclidian norm for continuous-time and discrete-time signals, respectively. Let us suppose that the information about the desired signal is represented by M sets, $C_m, \quad m = 1, 2, \ldots, M$. Since the desired signal satisfies all of the constraints it must be in the intersection set $C_o = \cap_{m=1}^{M} C_m$. Any member of the set C_o is called a feasible solution [7]. If all of the sets C_m are closed and convex then a feasible solution can be found by making successive orthogonal projections onto the sets C_m. Let P_m be the orthogonal projection operator onto the set C_m. The iterates defined by the following equation

$$\mathbf{y}^{(l+1)} \;=\; P_1 P_2 \cdots P_M \mathbf{y}^{(l)}, \quad l = 0, 1, 2, \ldots \tag{2.1}$$

converge to a member of the set C_o, regardless of the initial signal $\mathbf{y}^{(0)}$. The number of convex sets can be infinite. The rate of convergence can be improved by using

non-orthogonal projections as well. We do not devote further space to the underlying mathematical concepts, which can be found in [3].

2.2 Fractional Fourier Transform

In this section, the fractional Fourier transform is briefly reviewed and the signal recovery problem is formulated. The fractional Fourier transform (FRT) has found many applications in signal and image processing and optics [11–39]. The ath-order fractional Fourier transform operation corresponds to the ath power of the ordinary Fourier transform operation. The zeroth-order fractional Fourier transform of a function is the function itself and the first-order transform is equal to the ordinary Fourier transform. The relationship of the FRT to wave and beam propagation is well established [40–42]. It is well-known that the Fourier transform of the original object, aperture, or source distribution is observed in the far field. It has been shown that at closer distances, one observes the fractional Fourier transforms of the original object. As the wave propagates, its distribution evolves through FRTs of increasing order. In other words, it is continually fractional Fourier transformed as it propagates, starting from the original function and finally reaching its ordinary Fourier transform in the far field. Thus the problem of recovering signals from partial FRT information naturally finds applications in wave propagation problems where the measured information is partial, spread over several observation planes, or not of sufficient spatial resolution or accuracy. For a comprehensive treatment of the transform and its properties the reader is referred to [11].

Let us denote the ath-order fractional Fourier transform operator by $\mathcal{F}^a$. When $a = 1$ we have the ordinary Fourier transform operator $\mathcal{F}$. The FRT may be defined by standard eigenvalue methods for finding a function $G(\mathcal{H})$ of a linear operator $\mathcal{H}$. Hermite-Gaussian functions are the eigenfunctions of the ordinary Fourier transform: $\mathcal{F}\psi_n(u) = \exp(-jn\pi/2)\psi_n(u)$, where $\psi_n(u)$, $n = 0, 1, 2, \ldots$, are the set of Hermite-Gaussian functions: $2^{1/4}(2^n n!)^{-1/2} H_n(\sqrt{2\pi}\, u)\exp(-\pi u^2)$ and $H_n(u)$ are the standard Hermite polynomials. The fractional Fourier transform is defined in terms of the eigenvalue equation $\mathcal{F}^a\psi_n(u) = [\exp(-jn\pi/2)]^a\psi_n(u)$ with

the fractional ath power $[\exp(-jn\pi/2)]^a = \exp(-jan\pi/2)$. An analytic expression for the FRT of an arbitrary square-integrable function $x(u)$ can be obtained by expanding it in terms of the complete orthonormal set of functions $\psi_n(u)$ and then applying the above eigenvalue equation to each term of the expansion. This leads to the following expression for the ath order fractional Fourier transform $x_a(u) \equiv \mathcal{F}^a x(u)$ [11]:

$$x_a(u) = \sqrt{1 - j\cot(\frac{a\pi}{2})} \int_{-\infty}^{\infty} du' x(u') \cdot \exp\left\{j\pi\left[\cot(\frac{a\pi}{2})\, u^2 - 2\csc(\frac{a\pi}{2})\, uu' + \cot(\frac{a\pi}{2})\, u'^2\right]\right\} \tag{2.2}$$

The zeroth-order fractional Fourier transform of a function is the function itself. Positive and negative integer values of a simply correspond to repeated application of the ordinary forward and inverse Fourier transforms respectively. The fractional Fourier transform operator satisfies index additivity: $\mathcal{F}^{a_2}\mathcal{F}^{a_1} = \mathcal{F}^{a_2+a_1}$. The operator $\mathcal{F}^a$ is periodic in a with period 4 since $\mathcal{F}^2$ equals the parity operator which maps $x(u)$ to $x(-u)$ and $\mathcal{F}^4$ equals the identity operator.

The ath-order discrete fractional Fourier transform $\mathbf{x}_a$ of an $N \times 1$ vector $\mathbf{x}$ is defined as $\mathbf{x}_a = \mathbf{F}^a\mathbf{x}$, where $\mathbf{F}^a$ is the $N \times N$ discrete fractional Fourier transform matrix [47], which is essentially the ath power of the ordinary discrete Fourier transform matrix $\mathbf{F}$. Let the discrete-time vector $\mathbf{x}$ contain the samples of the continuous time signal $x(u)$. If N is chosen equal to or greater than the space-bandwidth product of the signal $x(u)$, then the discrete fractional transform approximates the continuous fractional transform in the same way as the ordinary discrete transform approximates the ordinary continuous transform.

Chapter 3

Pulse Shape Design

The problem of pulse shape design often comes up in communication systems including pulse amplitude modulation, frequency shift keying, and phase shift keying with the challenge of utilizing the bandwidth efficiently while having a low complexity receiver. One way is to use a suboptimal demodulator with a matched filter for complexity reduction and defining constraints on the spectrum, intersymbol interference, and duration of the pulse. Each of these conflicting constraints are convex sets in L^2, which are known to provide a useful base in optimization, laying ground for the method of projections onto convex sets [1–10]. This approach was previously used in designing pulse shapes for digital communication systems [46], where a communication without a matched filtering scheme is considered. However, the difficulty of associating the matched filter output to the corresponding time-domain signal still remains, which is a similar problem to phase retrieval [8, 43]. This information corresponds to a non-convex set in L^2. The autocorrelation function of the pulse is obtained by performing orthogonal projections onto convex sets corresponding to intersymbol interference, finite duration and spectral mask constraints, and we propose to find associated time-domain signals using linear phase signals or cepstral deconvolution.

The criteria of bandlimitedness, finite duration, and finite energy correspond to closed and convex sets in L^2 or ℓ^2 and they are widely used in various signal design and restoration problems [1–10]. The advantage of the method comes from

its convenient use and guaranteed convergence. At each step of the iteration, an orthogonal projection P_m is made onto a convex set C_m as:

$$x_p = P_m x = \arg\min \|x - x_m\| \,,\ x_m \in C_m \tag{3.1}$$

and the iterates defined by the equation:

$$y_{k+1} = P_1 P_2 \cdots P_M y_k \tag{3.2}$$

reaches a feasible solution, which is a member of the intersection $C_0 = \bigcap_{m=1}^{M} C_m$. Note that the feasible solution may not be unique. However, the intersection C_0 of the convex sets is also a convex set and at each step of the iterations we get closer to a solution, so that the convergence is guaranteed regardless of the initial iterate, when C_0 is nonempty.

In this thesis, we develop a design approach for finding a solution to the pulse shape design problem which satisfies bandwidth, duration, and intersymbol interference (interference due to other information bits) constraints. In the next section, we define the convex sets used in the pulse shape design problem and describe the iterative design algorithm.

3.1 Iterative Signal Design Algorithm

In this section, convex sets of autocorrelation functions corresponding to intersymbol interference (ISI) information, power spectrum, and duration constraints on the pulse shape are defined. Therefore, all desired properties of the pulse shape can be iteratively imposed as constraints on iterates defined by the POCS procedure. This approach leads to a globally convergent algorithm because all constraints correspond to closed and convex sets in ℓ^2. Once an autocorrelation function satisfying the constraints are obtained a time-domain pulse shape is estimated from the autocorrelation function determined by the POCS procedure. The estimated pulse-shape may be of infinite length. In this case, the tail of the time-domain signal is removed. This may lead to violation of some of the original constraints on the autocorrelation function. Therefore iterations are continued with the new autocorrelation function computed from the time-limited pulse shape.

Below are the convex sets defined for our design purposes. The convexity of these sets are shown in Appendix A.1.

Let $x[n]$ be the samples of the pulse shape and $r_x[k] = \sum_n x[n]x^*[n-k]$ be the corresponding autocorrelation function. The set C_1 is defined as the set of autocorrelation functions in ℓ^2 whose Fourier Transform is below a spectral mask $D(w)$:

$$C_1 = \left\{ \mathbf{r_x} \in \ell^2 \mid S_x(\omega) \leq D(\omega) \right\} \tag{3.3}$$

where S_x is the power spectrum of the pulse, or equivalently the Fourier transform of $r_x[k]$. This set represents a bound on the pulse energy.

Secondly, another convex set is defined by the time-limitedness of the signal by an interval of duration T_p. Thus, the corresponding autocorrelation function is also time-limited. When the pulse is nonzero for $[0, T_p]$, the corresponding autocorrelation function is possibly nonzero in the interval $[-T_p, T_p]$ and the convex set C_2 describing the time-limitedness information is defined as

$$C_2 = \left\{ \mathbf{r_x} \in \ell^2 \mid r_x[k] = 0,\ |kT_s| > T_p \right\} \tag{3.4}$$

where T_s is the discretization period of the underlying continuous signal.

Finally, we define the third convex set as the ℓ^2 signals whose autocorrelation samples at integer multiples of a period K (except 0^{th} sample) magnitude-wise sum up to less than a certain bound b. This corresponds to putting a bound on worst case degradation due to ISI. Formally,

$$C_3 = \left\{ \mathbf{r_x} \in \ell^2 \mid \sum_{k \neq 0} |r_x[k \cdot K]| \leq b,\ b > 0 \right\} \tag{3.5}$$

where $r_x[k] = \sum_n x[n] \cdot x^*[n-k]$ is the autocorrelation of the signal.

This way, we define three convex sets of autocorrelation functions, which we can use in a POCS framework. Furthermore, we need to use the fact that the Fourier transform of the autocorrelation function is real due to the conjugate symmetry of the autocorrelation function. The associated convex set with this property can be denoted by:

$$C_4 = \left\{ \mathbf{r_x} \in \ell^2 \mid S_x(\omega) \in \mathbf{R}, \forall \omega \in \mathbf{R} \right\} \tag{3.6}$$

Additionally, the autocorrelation function $r_x[k]$ has to have its maximum at $k = 0$. Without loss of generality, we can define another convex set with the assumption of a unit energy pulse, as follows:

$$C_5 = \left\{ \mathbf{r_x} \in \ell^2 \mid r_x[0] = 1;\ |r_x[k]| \leq 1, k \neq 0 \right\} \tag{3.7}$$

Next we describe the projection operators onto sets $C_1, \ldots, C_5$. The projection of a signal $r[k]$ onto the set C_1 is given by the following equation:

$$P_1 r[k] = \mathcal{F}^{-1} \left\{ S'(\omega) \right\} \tag{3.8}$$

where

$$S'(\omega) = \begin{cases} S(\omega), & |S(\omega)| \leq D\left(\omega\right) \\ D(\omega) \cdot e^{j\Phi(\omega)}, & \text{otherwise} \end{cases} \tag{3.9}$$

and $\Phi(\omega)$ is the phase of $S\left(\omega\right)$, and $S\left(\omega\right)$ is the Fourier transform of $r[k]$.

The projection of a signal $r[k]$ onto the set C_2 is given by:

$$P_2 r[k] = \begin{cases} r[k], & kT_s \in [-T_p, T_p] \\ 0, & \text{otherwise} \end{cases} \tag{3.10}$$

where T_s is the sampling period.

Although the following projection operator may not be orthogonal, a signal in C_3 corresponding to a given $r[k]$ can be obtained as follows:

$$P_3 r[k] = \begin{cases} \frac{b}{\sum\limits_{m \neq 0} |r[m \cdot K]|} \cdot r[k], & \sum\limits_{m \neq 0} |r\left[m \cdot K\right]| > b,\ k = m \cdot K, m \neq 0 \\ r\left[k\right], & \text{otherwise} \end{cases} \tag{3.11}$$

Note that the above operation leaves $r[0]$ unaltered.

Finally, projections of a signal $r[k]$ onto the sets C_4 and C_5 are given by the following equations, respectively:

$$P_4 r[k] = \mathcal{F}^{-1} \left\{ Re \left\{ \mathcal{F} \left\{ r[k] \right\} \right\} \right\} \tag{3.12}$$

and

$$P_5 r[k] = \begin{cases} r[k], & r[k] \leq 1, k \neq 0 \\ \frac{r[k]}{|r[k]|}, & \text{otherwise} \end{cases} \tag{3.13}$$

The orthogonality of the projection operators in Equations (3.8),(3.10),(3.12), and (3.13) are shown in Appendix A.2. Using the projection operators $P_1, P_2, \ldots, P_5$ onto the convex sets $C_1, C_2, \ldots, C_5$, we can define a globally convergent iterative scheme as in Equation 3.2 for finding an autocorrelation function. However, we still need to find the time-domain signal associated with the autocorrelation function.

Although we can achieve a conjugate symmetric function time-limited between $[-T_p, T_p]$ satisfying

$$\begin{array}{ll} |r_x[k]| < 1, & k \neq 0 \\ r_x[k] = 1, & k = 0 \end{array}, \tag{3.14}$$

we can not guarantee that the resulting autocorrelation sequence belongs to a time-limited signal. For example, when we apply cepstral deconvolution to the resulting r_x in order to find a minimum phase solution, we may not achieve a time-limited function which has the same autocorrelation function.

To obtain a finite extent signal, we modify the iterative POCS procedure in two ways. It is important to note that these modifications may eliminate the property of global convergence, however, this approach helps find an association between the time domain signal and the autocorrelation function. In the first case, a linear phase component is added to the square root of the spectrum after projecting the current interate onto the sets $C_1, C_2, \ldots, C_5$. Let the l^{th} iterate be $r_x^{(l)}[k]$. The signal $x^{(l)}[n]$ is obtained as:

$$x^{(l)}[n] = \mathcal{F}^{-1}\left\{\sqrt{\mathcal{F}\left\{r_x^{(l)}[k]\right\}} \cdot e^{-j\omega n_0}\right\} \tag{3.15}$$

where $S_x^{(l)}(\omega) = \mathcal{F}\left[r_x^{(l)}[k]\right]$ and n_0 is a nominal time delay for ensuring realizability [44]. The signal $x^{(l)}[n]$ may turn out to be of infinite length. So it is forced to be a finite extent signal as follows

$$x^{(l)}[n] = \begin{cases} x^{(l)}[n], & nT_s \in [0, T_p] \\ 0, & \text{otherwise} \end{cases} \tag{3.16}$$

Next, a new autocorrelation sequence is obtained from $x^{(l)}[n]$ described as:

$$r_x^{(l+1)}[k] = \sum_n x^{(l)}[n] \cdot x^{(l)^*}[n-k] \tag{3.17}$$

and it is used in the next iteration cycle of the POCS scheme. The above iterations described in Equations (3.15),(3.16), and (3.17) need not be carried out in every

iteration cycle. It can be implemented afer a reasonable $r_x^{(l)}[k]$ satisfying (or almost satisfying) Fourier domain constraints is obtained.

Our second approach is based on cepstral deconvolution. A minimum phase signal is obtained after projecting the current iterate onto the sets $C_1, C_2, \ldots, C_5$. Let the current iterate be denoted by $r_x^{(l)}[k]$. The minimum phase signal $x_m^{(l)}[n]$ is defined as [45]:

$$x_m^{(l)}[n] = \mathcal{F}^{-1}\left\{\exp\left[\mathcal{F}\left\{H\left(\mathcal{F}^{-1}\left\{\ln \mathcal{F}\left\{r_x[k]\right\}\right\}\right)\right\}\right]\right\} \tag{3.18}$$

where

$$Hx_c[n] = \begin{cases} 0, & n < 0 \\ \frac{x_c[0]}{2}, & n = 0 \\ x_c[n], & n > 0 \end{cases} \tag{3.19}$$

is the operator which takes the causal part of the cepstrum $x_c[n]$. The resulting minimum phase signal may also be of infinite length. So it is forced to be a finite extent signal as follows

$$x_m^{(l)}[n] = \begin{cases} x_m^{(l)}[n], & nT_s \in [0, T_p] \\ 0, & \text{otherwise} \end{cases} \tag{3.20}$$

Similar to the previous approach, a new autocorrelation sequence is obtained from

$$r_x^{(l+1)}[k] = \sum_n x_m^{(l)}[n] \cdot x_m^{(l)^*}[n-k] \tag{3.21}$$

and it is used in the next iteration cycle of the POCS scheme.

In the next section, we illustrate the design approach with some examples.

3.2 Design Examples

In this section, we present some exemplary design approaches through our method. The definition of the pulse shape design problem is as follows: We want to design a pulse shape that is below a spectral mask in frequency domain, can be used with a matched filtering demodulation scheme not causing a worst case degradation

in signal-to-noise ratio due to intersymbol interference more than a certain value, yields a certain communication rate, and is also finite duration. The spectral mask and pulse duration used in the following design examples remain constant, while we use several different values of SNR degradation (bound on ISI) and rate of communication. In each example, we modify these constraints in order to illustrate the tradeoffs between them. We first use the method associated with finding the linear phase signal as given in Equation (3.11). In order to achieve a feasible solution quickly, we start from an initial root raised-cosine signal with roll-off factor $\alpha = 1$. Although this is not a part of the conventional procedure, we are aware of a signal (root raised-cosine) which is somewhat close to satisfying our requirements; and we simply use that fact by making the root raised-cosine signal our starting point.

First we identify the values that result in the worst case degradation for the k^{th} bit as:

$$I_k(j) = \begin{cases} 1, & r_x(|j-k|\,T) > 0 \\ 0, & \text{otherwise} \end{cases}, \; j \neq k \tag{3.22}$$

where T is the sampling interval of the matched filter output. This is simply because the intersymbol interference term should be the negative of the matched filter output at zero lag, for the worst case degradation to occur.

Then we can define the worst case ISI for a unit energy pulse shape $x(t)$ as:

$$ISI = \sum_{k \neq 0} |r_x(kT)| \tag{3.23}$$

for which the degradation in signal-to-noise ratio (SNR) is:

$$d = -20\log_{10}(1 - ISI) \tag{3.24}$$

Note that $d' = -20\log_{10}(1 + ISI)$ is not the worst case degradation since $d' < d$, $ISI > 0$. Placing a constraint on the worst case degradation $d < 0.25$ dB directly puts a bound on the ISI as:

$$-20\log_{10}(1 - ISI) < 0.25 \Longrightarrow ISI < 1 - 10^{-\frac{0.25}{20}} \tag{3.25}$$

which constitutes the b value in (3.11). Henceforth, we apply the iterative scheme proposed in the previous section.

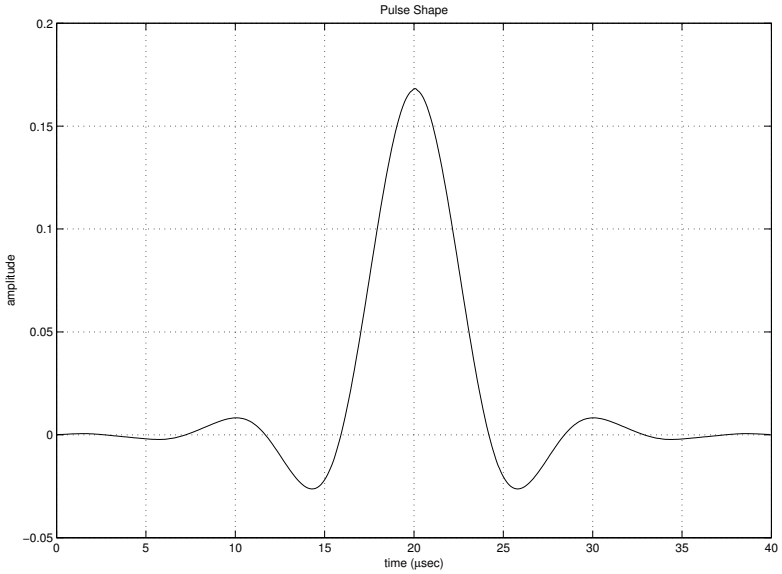

Figure 3.1: Linear phase pulse shape designed via proposed method

To achieve the outcome of successive projections onto the sets we defined in the previous section, we stop the iterations immediately as we reach a feasible solution. The pulse shape given below in Fig. 3.1 yields a symbol rate of 218 kHz, causing a worst case degradation less than 0.25 dB, with a pulse duration of 40 μsec.

Fig. 3.2 illustrates the matched filter output at the receiver, and the power spectrum of the designed pulse. The mask is nowhere exceeded by the pulse spectrum, as expected.

In our second design approach, we take the minimal phase root and therefore apply the corresponding operations defined in the previous section. The initial iterate was chosen to be random. Below is the pulse shape in Fig. 3.3 and the matched filter output, spectral mask and power spectrum of the pulse in Fig. 3.4. In order to improve the speed of convergence, we specified tighter bounds in the projection onto the spectral mask set. In this case the worst case degradation in SNR turned out to be 1.75 dB. We observe the tradeoff between speed of convergence (projection with a tighter spectral mask) and the worst case degradation in SNR

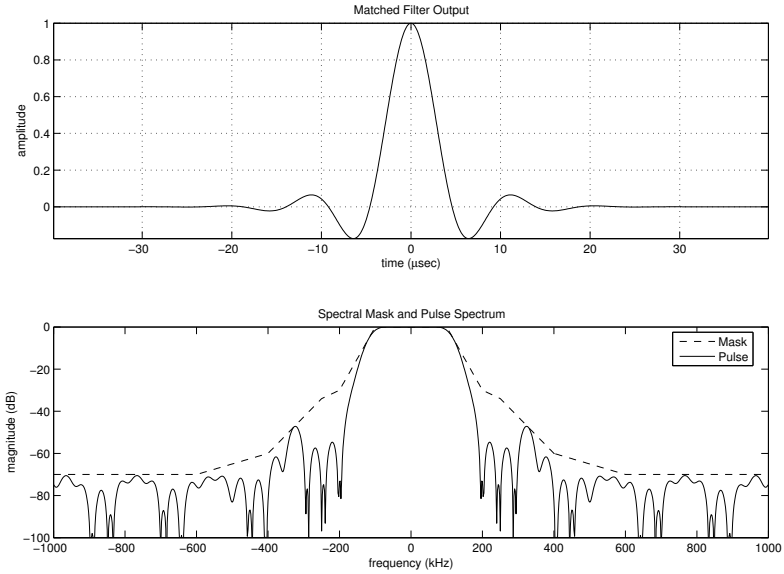

Figure 3.2: a) Matched filter output, b) Spectral mask and pulse spectrum

due to ISI. Since we make the projections onto a narrower set defined by a tighter constraint, the intersection set also gets narrower; hence, we can only achieve a lower SNR with the resulting pulse shape.

Figures 3.5-3.10 illustrate two other pulse shapes in time-domain, their auto-correlation functions, and their spectral characteristics, respectively. The pulses designed with this method yields a bit rate of 228 kHz (Fig. 3.5) and 234 kHz (Fig. 3.6), respectively, with a worst case degradation of 0.5 dB.

In all the examples, the iterates converged in about 10000 cycles, making the design algorithm convenient for implementation on an ordinary personal computer. Figures 3.11-3.12 illustrate the square error between the pulse spectrum and the spectral mask for the first two pulse shapes. The error appears to increase after an initial abrupt decrease. This is due to the negative error (where the pulse spectrum is below the spectral mask), even if the iterates get closer to a feasible solution, error defined this way may increase.

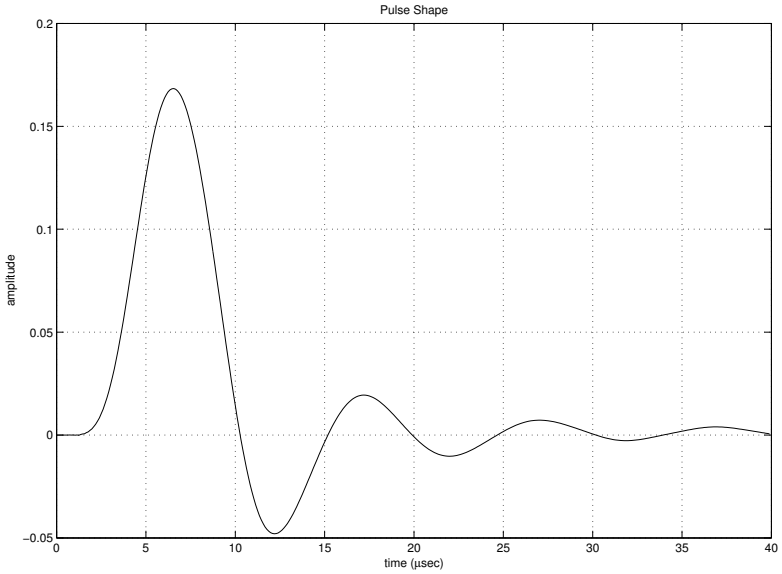

Figure 3.3: Minimum phase pulse shape

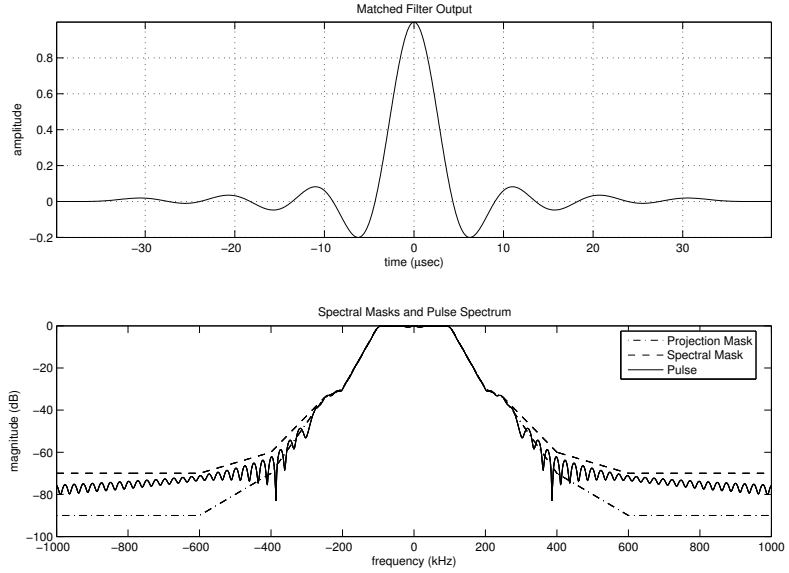

Figure 3.4: a) Matched filter output, b) Spectral mask used in projections (dashdot), spectral constraint mask (dash), power spectrum of the pulse (solid)

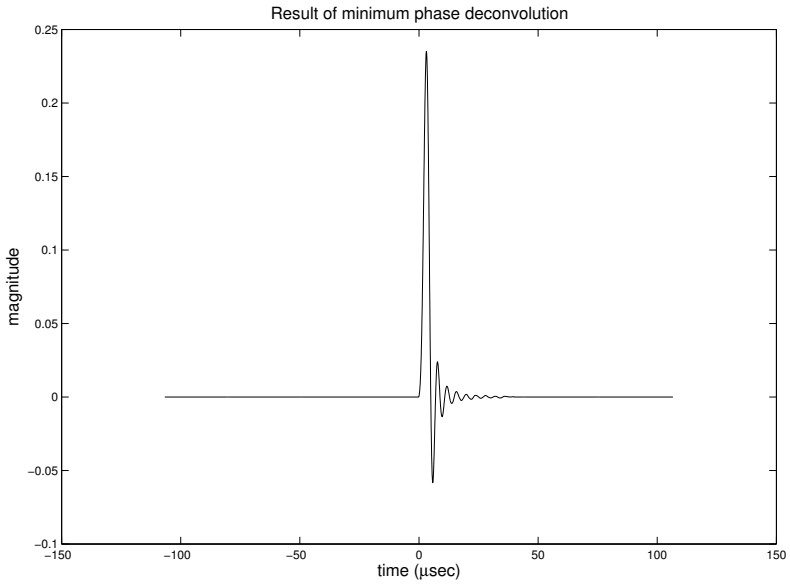

Figure 3.5: Minimum phase pulse shape that yields a bit rate of 228 kHz

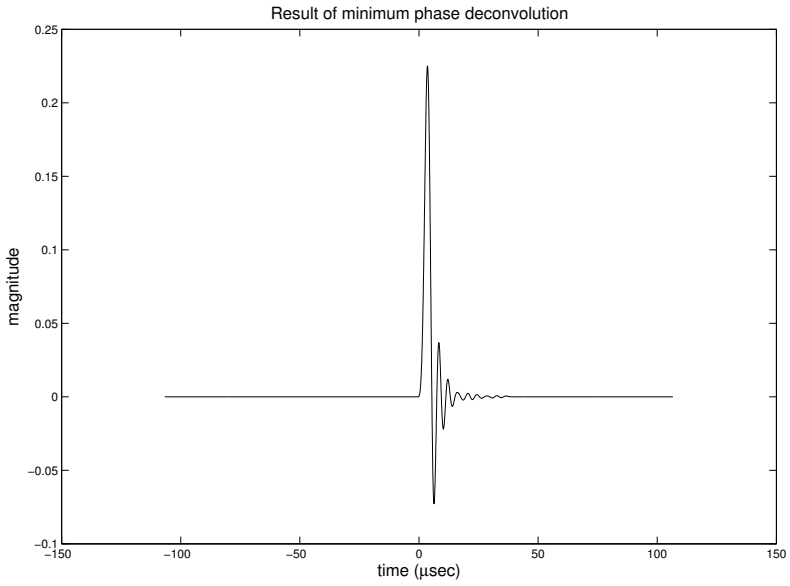

Figure 3.6: Minimum phase pulse shape that yields a bit rate of 234 kHz

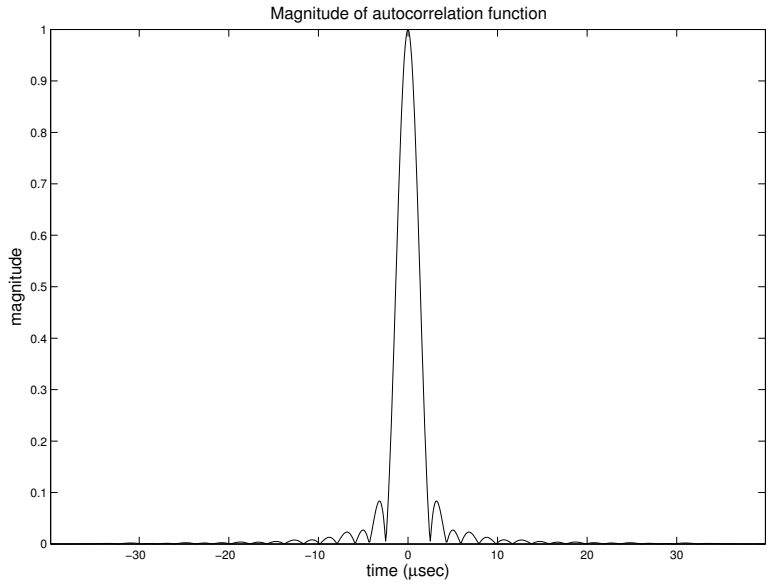

Figure 3.7: Autocorrelation function of the pulse with 228 kHz bit rate

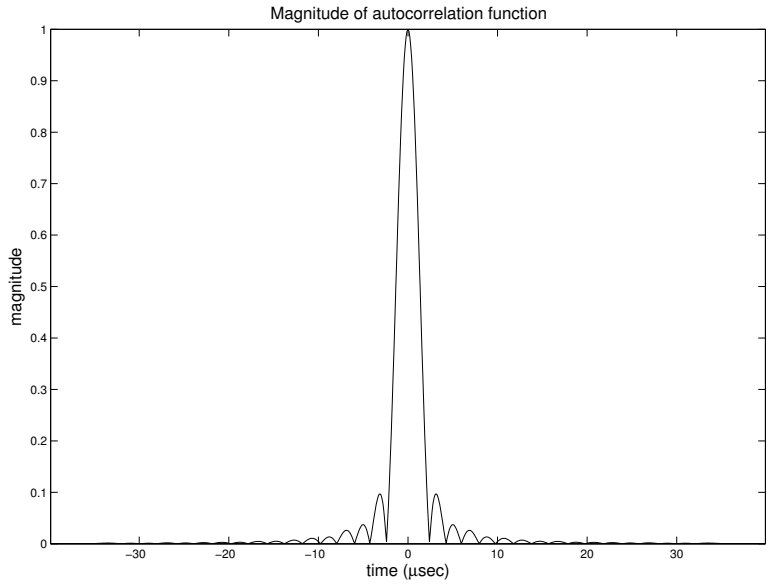

Figure 3.8: Autocorrelation function of the pulse with 234 kHz bit rate

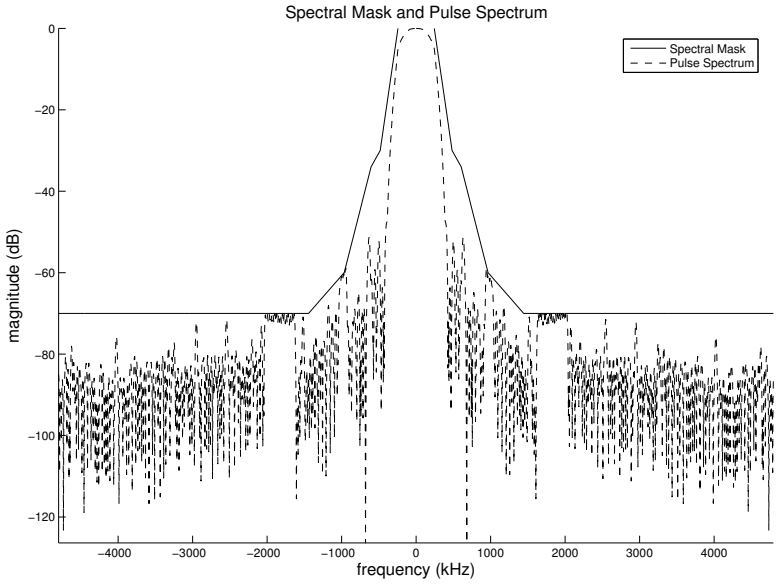

Figure 3.9: Spectral mask (solid) and spectrum of the pulse with 228 kHz bit rate (dash)

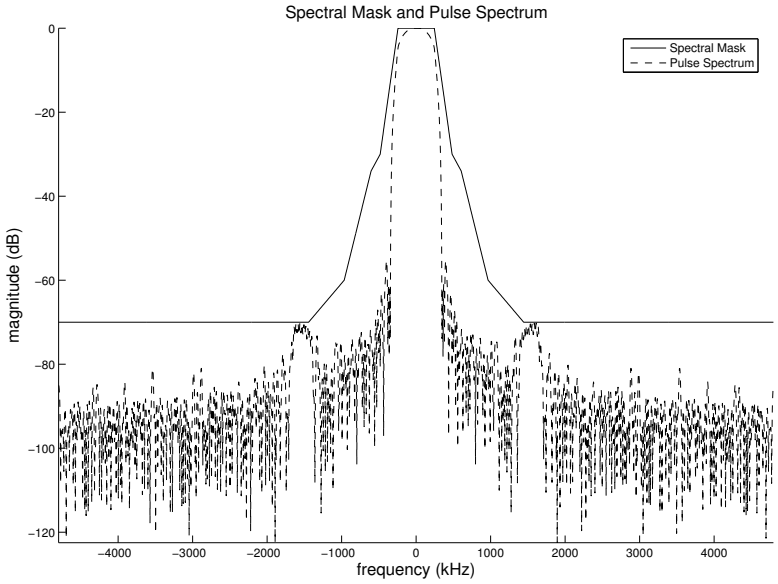

Figure 3.10: Spectral mask (solid) and spectrum of the pulse with 234 kHz bit rate (dash)

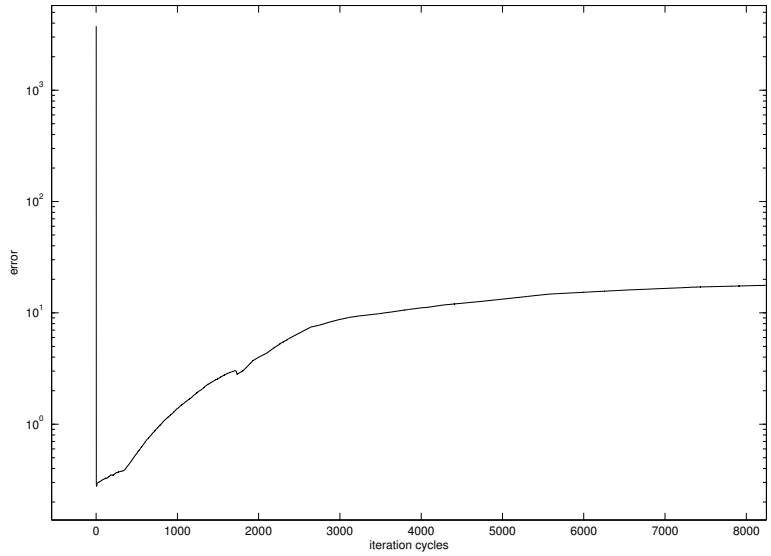

Figure 3.11: Square error vs iteration cycles for the pulse shape in Fig. 3.1

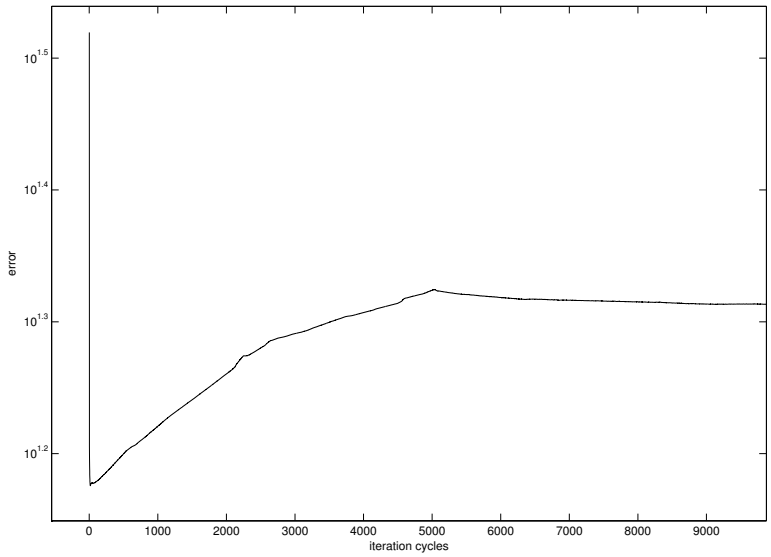

Figure 3.12: Square error vs iteration cycles for the pulse shape in Fig. 3.3

3.3 Discussion and Conclusion

In this part of the thesis, we present a method for designing pulse shapes that obey certain constraints defined in time and frequency domains. Other constraints that can be represented as convex sets can be included in the procedure, as well. In order to find time-domain signals satisfying bandwidth, ISI, and duration constraints, we define convex sets of autocorrelation functions and associate them to time-domain signals within iterative projections. This association comes with a possible compromise of the global convergence propery. However, we are able to find feasible solutions for various criteria in our design examples which illustrate the procedure.

Although not investigated in this thesis, the set given in Equation (3.5) can be extended to include more index values, particularly in the neighboring intervals of the sampling times, in order to reduce possible degradation due to sampling jitter. This approach may provide robustness against sampling jitter as well. Here, we only considered the intersymbol interference due to other information bits.

In our examples iterations converged in reasonable numbers of cycles, satisfying all of the requirements. When the constraints are defined to be too tight, the algorithm oscillates between the projections on the constraint sets, which have an empty intersection set. In this case, one should restart the procedure with looser constraints, until the intersection of the constraint sets is nonempty. Also, defining the constraints a little tighter than necessary improves the speed of convergence, with a compromise between finding the minimum mean square distance solution, a higher degradation in SNR occurs as a result.

Chapter 4

Signal Recovery from FRT Information

The signal recovery problem under consideration is the reconstruction of $x(u)$ from $x_a(u),\ u \in\ U \subset \mathbf{R}$, at one or more domains $a = a_1, a_2, \ldots$. The set U may consist of the union of an arbitrary collection of bands (intervals) in the ath fractional Fourier domain. It may also contain or consist of isolated discrete points representing measurements of $x_a(u)$ at $u = u_i,\ i = 1, 2, \ldots$. As in the case of signal recovery from partial ordinary Fourier transform information, the reconstruction problem is very noise sensitive in the event that U represents a narrow band in the ath FRT domain.

4.1 Iterative Signal Recovery Algorithm

This section presents the signal recovery algorithm which is devised by using the method of projections onto convex sets (POCS) [1–3] that has been successfully used in many signal recovery and restoration problems [5–10, 48]. The key idea is to obtain a solution which is consistent with all the available information. In this method the set of all possible signals is assumed to constitute a Hilbert space with an associated norm in which the prior information about the desired signal can be

represented in terms of convex sets. In this thesis, the Hilbert space is L^2 or ℓ^2 with Euclidian norm for continuous-time and discrete-time signals, respectively. Let us suppose that the information about the desired signal is represented by M sets, $C_m, \quad m = 1, 2, \ldots, M$. Since the desired signal satisfies all of the constraints, it must be in the intersection set $C_o = \cap_{m=1}^{M} C_m$.

We define the set C_1 in L^2 as the set of signals whose a_1th fractional Fourier transforms are equal to $\hat{x}_{a_1}(u)$ in the band $u \in U$ in the a_1th fractional domain.

$$C_1 \stackrel{\Delta}{=} \{\mathbf{x} \ : \ x_{a_1}(u) = \hat{x}_{a_1}(u), \quad u \in U\} \tag{4.1}$$

This set is convex because the integral operator in Equation (2.2) is a linear operator. The proof of closedness can be established as in [1]. If data is also available in another a_2th fractional domain, another set C_2 can be defined in a similar manner, and so on. If the signal is a finite extent signal then this information can be modeled as a closed and convex set as in other well-known signal recovery problems. Actually, time/space-domain information about the original signal including the knowledge that $x(u) = 0$ in a bounded or unbounded window in the time/space domain already belongs to the above class of sets since the time/space-domain merely corresponds to the special case of $a = 0$. Equation (2.2) simply becomes the identity operator for the fraction $a = 0$.

Partial information in the discrete fractional Fourier domains can be represented as convex sets in ℓ^2:

$$C_d \stackrel{\Delta}{=} \{\mathbf{x} \ : \ x_a[n] = \hat{x}_a[n], \quad n \in U_d\} \tag{4.2}$$

where U_d is a set of discrete index points.

Another convex set which can be used in the signal recovery algorithm is the bounded energy set, C_e which is the set of sequences whose energy is bounded by ϵ_o, i.e.,

$$C_e \stackrel{\Delta}{=} \{\mathbf{x} \ : \ ||\mathbf{x}||_2^2 \ \leq \ \epsilon_o \ \} \tag{4.3}$$

This set provides robustness against noise, if ϵ_o is known or some idea about ϵ_o is available. Yet other convex sets describing partial fractional Fourier domain information can be defined. Non-negativity information about the signal samples also

leads to a closed and convex set C_p in ℓ^2 or L^2 [1, 2]. The same also holds when we know that the signal is real. The key operation of the method of POCS is the orthogonal projection onto a convex set. Projection operations onto the sets $C_1, C_2, ..., C_K$ are straightforward to implement. Let $x^{(l)}(u)$ be the lth iterate of the iterative recovery process. Let $x_a^{(l)}(u)$ be fractional Fourier transform of $x^{(l)}$ in the ath domain. The projection operator replaces the fractional Fourier transform values of $x_a^{(l)}(u)$ in the band U

$$x_a^{(l+1)}(u) = \hat{x}_a(u), \quad u \in U, \tag{4.4}$$

where $\hat{x}_a(u)$ is the known fractional Fourier transform in the ath domain and the projection operator retains the rest of the data outside the band U:

$$x_a^{(l+1)}(u) = x_a^{(l)}(u), \quad u \notin U. \tag{4.5}$$

Projection onto the energy set C_e is described in [3]. It simply consists of scaling the signal $x(u)$ such that the energy of the scaled signal is ϵ_o. Projection onto the non-negativity set C_p is carried out by simply forcing the negative values of $x(u)$ to zero.

Let us now summarize the signal recovery algorithm from partial fractional Fourier transform information. The algorithm starts with an arbitrary initial estimate $\mathbf{y}(0) \in L^2$. The initial estimate $\mathbf{y}_0$ is successively projected onto the sets C_m, $m = 1, 2, \ldots, M$, representing the partial fractional Fourier domain information in domains a_m, $m = 1, 2, \ldots, M$ by using Equations (4.4) and (4.5). The order of projections is immaterial [3]. In this manner the first iteration cycle is completed and the Kth iterate $\mathbf{x}^{(K)}$ is obtained. If energy and/or non-negativity information is available then the current iterate is also projected onto the set C_e and/or C_p. This iterative procedure is repeated until a satisfactory level of error difference in successive iterations is obtained.

4.2 Application Examples

The problem formulated and solved in this thesis is very general and encompasses a variety of application scenarios. In this section we will present several such prototypical application scenarios and examples; other variations can be easily imagined. To rephrase the general problem, it is assumed that measurements $x_a(u)$ at $u = u_i,\ i = 1, 2, \ldots, I_a$ for $a = a_j,\ j = 1, 2, \ldots$ are available. This may also include the assumption that the signal is of finite support. Non-negativity and/or realness information may be additionally available. The fractional Fourier transform integral (1) is either numerically approximated or, if the fractional Fourier domain data is available on a uniform grid, the problem can be directly posed in terms of the discrete fractional Fourier transform. The latter is assumed in the following examples.

Scenario 1: *Low-resolution version of signal is available in the FRT domain together with finite-extent information.* [49]

In the examples we consider, it is known that the desired signal is zero outside a certain interval, and only one out of every three samples in the fractional Fourier domain are known over a certain extent.

We assume that the $N = 128$ point discrete fractional Fourier transform $x_{0.5}[n]$ of the desired signal $\mathbf{x} = \{0, \ldots, 0, \underset{\uparrow}{1}, 2, 3, 2, 1, 3, 3, 1, 1, 1, 3, 3, 1, 2, 3, 2, 1, 0, \ldots, 0\}$ defined in the interval $-64 \leq n < 64$, is available for $n = -64, -61, -58, \ldots, 59, 62$. It is also known that $x[n] = 0$ outside the interval $-5 \leq n < 25$. We define percentage restoration error as follows: $100 \times ||\mathbf{x}^{(l)} - \mathbf{x}||^2/||\mathbf{x}||^2$ where $\mathbf{x}^{(l)}$ is the lth iterate. In this example (1a), the percentage error drops below 1% after 25 iterations, a result which may be sufficient for many applications. However, in this example further iterations reduce the error only marginally, since the available information is not sufficient to uniquely recover the signal; a signal close but not identical to the original signal is obtained. The iterates converge to a member of the set C_o which is the intersection of all the sets used in the reconstruction process.

Let us consider a variation of this example where the available information allows

the recovery of the original signal with a much higher accuracy (1b). We assume the fractional Fourier domain information about the original signal is the same as above but the available time-domain information about the signal is that $x[n] = 0$ for $n < 0$ and $x[n]$ is everywhere real. In this case, the error drops below 0.0001% after 200 iterations.

Let us now consider the same example as in 1a, but add stationary zero-mean Gaussian white noise onto the measured fractional Fourier transform data, with a signal-to-noise ratio of unity. Due to the substantial amount of noise, the iterates fluctuate around the solution, and the percentage error does not fall below 2%.

Scenario 2: *Low-resolution version of signal is available in two different FRT domains, possibly with additional information.* [49]

In the examples we consider, only one out of every two samples of the FRT at two or three domains is known.

First we assume that we have all odd samples of $x_{0.5}[n]$ for $-64 \leq n < 64$ and all even samples of $x_{0.75}[n]$ for $-64 \leq n < 64$. In this example (2a), the error falls below 1% after 50 iterations and falls near 0.01% after 500 iterations.

In the next example (2b), odd samples of $x_{0.5}[n]$ and $x_{0.75}[n]$ are available within a limited range $-25 \leq n < 25$. Additionally we have all even samples of $x[n]$ for $-64 \leq n < 64$. This time, even after 500 iterations, the error is reduced only to around 2-3%. This relatively large error is not surprising since the available information, in terms of the number of available complex samples, is not sufficient to specify a unique solution.

If we additionally know that the signal is zero outside the interval $-32 \leq n < 32$, performance is much improved and in this case (2c), the error falls below 0.0001% after 100 iterations.

Scenario 3: *The FRT of the signal is known over a limited interval in a single domain, together with additional constraints.*

In the example we consider (3a) the signal is known at full resolution in the 0.3rd

fractional domain over the interval $-15 \leq n < 15$. We additionally know that the original signal in the time/space domain is real. The error drops below 0.1% after 100 iterations.

Scenario 4: *The FRT of the signal is known over a limited interval in two or more domains, possibly with additional constraints.*

First we assume (4a) that $\mathbf{x}_{0.5}[n]$ is known in the interval $0 \leq n < 55$ and $\mathbf{x}_{0.75}[n]$ is known in $-55 \leq n < 0$. The error drops below 0.1% after 100 iterations.

Next, we consider the case where the signal is known over a rather small interval in several domains (4b). The signal is known in the 0.2nd, 0.3rd, 0.5th, 0.6th, 0.75th domains in the interval $-5 \leq n < 5$ and we additionally know that $x[n]$ takes real values for all n. The error drops below 0.5% after 100 iterations.

Finally, to further illustrate the application of the method, we consider the case of a finite extent radar pulse corrupted by wideband chirp interference. The time-domain radar pulse $x[n]$ and the interference term $y[n]$ are given by (Fig. 4.1):

$$x[n] = \frac{1}{\sqrt{1600\pi}} \exp\left[-\frac{n^2}{1600} + j\frac{\pi n^2}{256}\tan\left(0.2\frac{\pi}{2}\right)\right], \tag{4.6}$$

$$y[n] = \frac{1}{\sqrt{4\pi}} \exp\left[-\frac{n^2}{400} + j\frac{\pi n^2}{256}\tan\left(-0.6\frac{\pi}{2}\right)\right], \tag{4.7}$$

for $-128 \leq n < 128$. The Wigner distribution of the corrupted signal is shown in Fig. 4.2, where we can clearly see the distribution of energy of $x[n]$ and $y[n]$. We will employ the following strategy to recover the radar pulse. Recall that the axis making angle $a\pi/2$ with the time/space axis is the ath fractional Fourier domain. Both the desired radar signal and the corrupting signal exhibit different degrees of compactness in different domains. Therefore we may transform to domains where their separation is relatively large and eliminate those parts which are heavily corrupted by the distorting signal and then use interpolation to recover the complete signal. We will make use of two domains, the domain in which the desired signal is maximally spread, and the domain in which it is most compact. The domain in which the desired signal is maximally spread is $a = 0.2$, and the corrupted signal in this domain is shown in Fig. 4.3. We will eliminate the corrupted interval $-24 \leq n < 24$ from this data and assume that the 0.2nd FRT of the signal is known only outside

this interval, in addition to the support information $x[n] = 0, |n| \geq 75$. Second, we look at the -0.8th domain in which the desired radar pulse is most compact, shown in Fig. 4.4. Here we know that the desired signal is of negligible value outside the interval $-4 \leq n < 4$ so that we will assume the -0.8th fractional Fourier transform of the signal is zero outside this interval. The signal is assumed not to be known inside the interval $-4 \leq n < 4$. The available information in the two domains now fulfills scenario 4 and the signal can be recovered by the interpolation procedure presented in this chapter of the thesis. The error falls to 0.2% after 200 iterations.

We also solved the same problem after adding additive zero-mean white Gaussian random noise to the corrupted radar pulse in the original $a = 0$th domain. The noise variance is $(0.002)^2$, which leads to noise sample values comparable to the uncorrupted signal. The error falls to around 2-3% after 50 iterations.

Although not used in this example, two additional domains could have been employed: (i) The domain in which the distorting signal is maximally distributed; here we would have eliminated all samples outside of a centrally located interval. (ii) The domain in which the distorting signal is most compact; here we would have eliminated the centrally located interval where the distorting signal is dominant.

4.3 Discussion and conclusion

In this part of the thesis, we present an iterative algorithm for signal recovery from partial fractional Fourier transform domain information. This problem finds applications in wave and beam propagation problems where the measured information is partial, spread over several observation planes, or not of sufficient spatial resolution. The signal recovery algorithm is developed by using the method of projections onto convex sets and convergence is assured regardless of the initial estimate. After presenting the general formulation, we presented several generic application scenarios illustrating a wide variety of prototypical situations which are covered by our framework. We also presented an application example involving the recovery of a

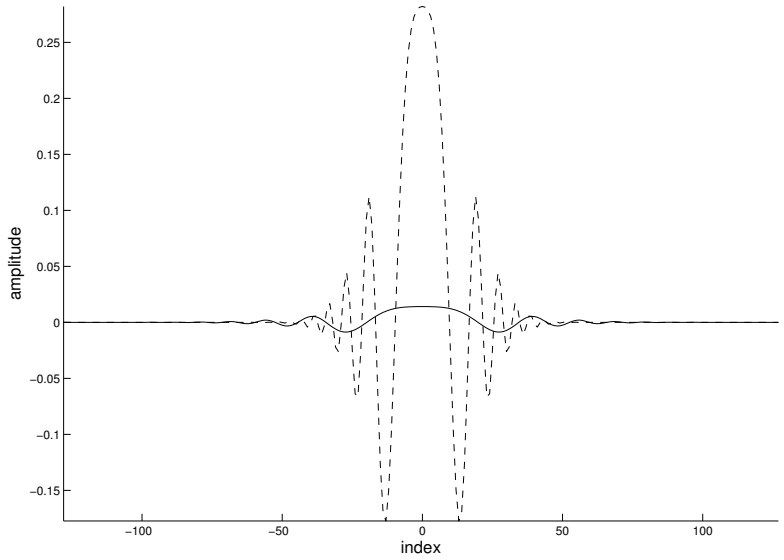

Figure 4.1: Real parts of the time-domain radar pulse and interference signal: radar pulse (solid line), interference signal (dashed line).

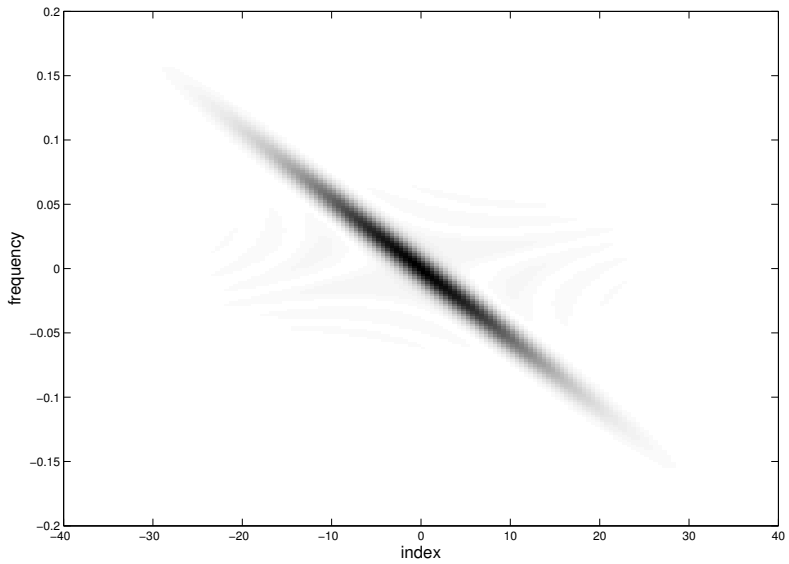

Figure 4.2: Wigner distribution of the corrupted signal.

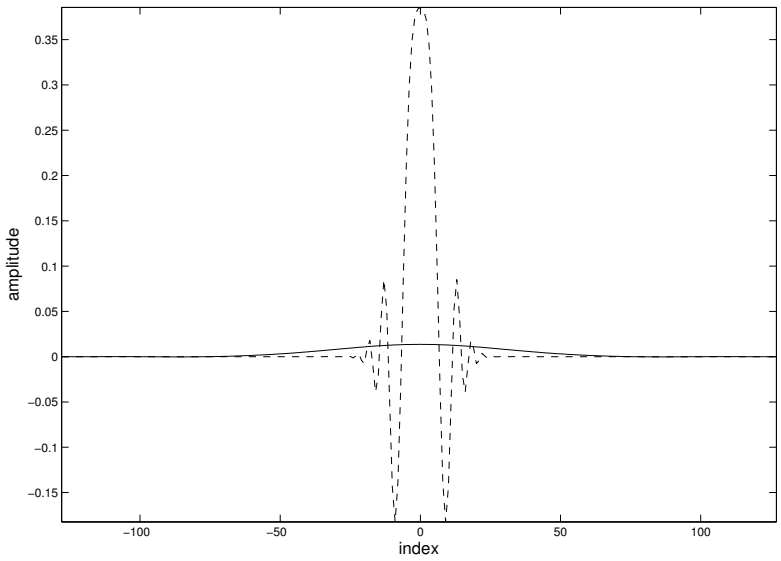

Figure 4.3: Real parts of the 0.2nd fractional Fourier transforms of the radar pulse and interference signal: radar pulse (solid line), interference signal (dashed line).

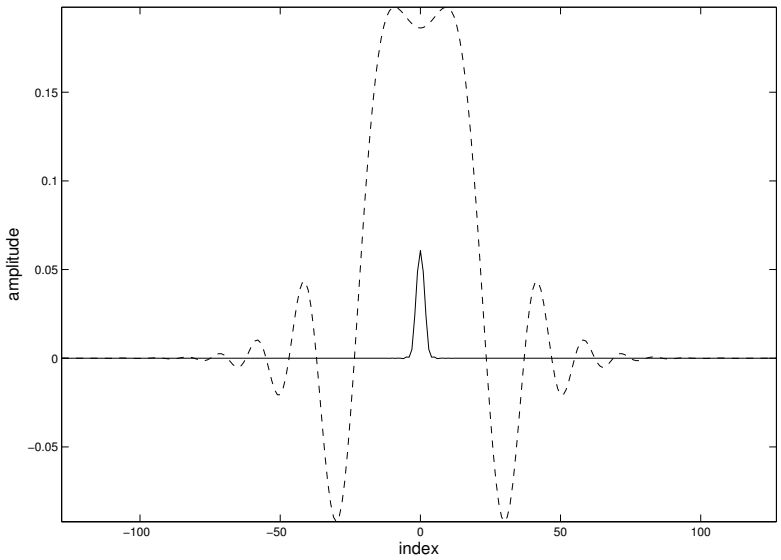

Figure 4.4: Real parts of the -0.8th fractional Fourier transforms of the radar pulse and interference signal: radar pulse (solid line), interference signal (dashed line).

corrupted radar pulse. The presented signal recovery technique can be easily extended to multi-dimensional problems as well. It can also be generalized to the case where signal information is available or can be deliberately measured in a number of generalized "domains" which are related through linear transformations other than the FRT, such as the family of linear canonical transforms [51].

In all the examples considered we have observed consistent behavior of the algorithm. If the FRT measurements are available in a very narrow interval, the corresponding entries of the neighboring rows of the transform matrix may get very close to each other and this structure may lead to unstable reconstruction results from noisy measurements. This is not especially related to the FRT case; in this respect, the problem is very similar to the problem of signal reconstruction from narrow-band ordinary Fourier transform information.

The relative overlap and separation of signal and noise (desired and undesired information), the localization of this overlap, and therefore the signal-to-noise ratio at a certain interval will in general be different in different domains. By choosing regions in each domain where the signal-to-noise ratio is relatively favorable and discarding those regions where it is unfavorable and then using the generalized interpolation strategy presented in this thesis to combine these partial signals, is a general approach which we believe will find widespread applicability in a variety of situations.

Chapter 5

Conclusions and Future Work

5.1 Conclusions

In this thesis, we investigated some applications of projections onto convex sets in signal design and recovery problems. We applied the method to the pulse shape design problem in communication scenarios with matched filtering, where intersymbol interference, spectral mask, and finite duration constraints are imposed on the pulse shape to be designed. We modeled these mathematical properties as convex sets, and we used a POCS framework in order to find a solution to the signal design problem. The problem of associating the autocorrelation function with a time-domain signal still persists. Nevertheless, we get around the problem by defining association rules with linear or minimum phase signals. Secondly, we apply the method of POCS to fractional Fourier transform domains, where partial information in different bands correspond to closed and convex sets. Accordingly, we define an iterative scheme for signal reconstruction from partial information in fractional Fourier domains. The method is globally convergent and straightforward to implement as compared to possible analytical approaches such as minimum mean square error, etc. We presented several prototypical scenarios and application examples to the signal design and recovery problems.

5.2 Future Work

As a future work on the pulse shape design problem, a mathematical set of constraints that define a legitimate autocorrelation function are to be sought. If one can define a convex set which consists of the autocorrelation functions with an exact root in time-domain, the procedure will become globally convergent and one can guarantee finding a solution given that there exists at least one.

Possible extensions of the signal recovery framework investigated in this thesis are:

1. Reconstruction of signals where measurements are made over an arbitrary curve on the propagating field. In fact, this is nothing but a special case of the general procedure defined in Chapter 4. Another interesting problem is the reconstruction of the field from random point measurements over the field, which finds application with swarm robots. Due to the nature of these problems, the iterative signal recovery method is suitable for use in their solutions.

2. Unification of the interpolation and phase retrieval problems. Phase retrieval problem appears in areas such as optics, astronomy, and cryptography. Due to the non-convex nature of the problem, it is more difficult to obtain a solution and convergence is not guaranteed in many cases. There may be some advantage in generalizing the problem to fractional Fourier domains together with the interpolation issue. Iterative methods remain promising due to their ability of incorporating a diverse set of information to find a solution.

Appendix A

Additional material on Chapter 3

A.1 Convexity of Sets

In this section of the appendix, we prove that the sets given in Equations (3.3-3.7) are convex. We will use the following definition of convexity throughout this section:

Definition 1. *A set C is convex if:*

$$\forall\, \mathbf{x}, \mathbf{y} \in C \Rightarrow \alpha\mathbf{x} + (1-\alpha)\mathbf{y} \in C \tag{A.1}$$

where $0 < \alpha < 1$.

Now we present the propositions and their proofs on the convexity of the sets given in Equations (3.3-3.7).

Proposition 1. *The set C_1 defined in Equation (3.3) is convex.*

Proof. For any $\mathbf{x}, \mathbf{y} \in C_1$, the Fourier transforms $\mathbf{X}, \mathbf{Y}$ of $\mathbf{x}, \mathbf{y}$ will have the following relationship:

$$\begin{aligned} \alpha X(\omega) + (1-\alpha)Y(\omega) &\leq \alpha D(\omega) + (1-\alpha)D(\omega) && \text{(A.2)} \\ &= D(\omega) && \text{(A.3)} \end{aligned}$$

and due to the linearity of the Fourier transform, we have

$$\alpha\mathbf{x} + (1-\alpha)\mathbf{y} \in C_1 \tag{A.4}$$

Hence, C_1 is convex. □

Proposition 2. *The set C_2 defined in Equation (3.4) is convex.*

Proof. For any $\mathbf{x}, \mathbf{y} \in C_2$, we have:

$$x[k] = y[k] = 0,\ k \geq N \tag{A.5}$$

where $N = \left\lfloor \frac{T_p}{T_s} \right\rfloor$. Then,

$$\alpha x[k] + (1-\alpha)y[k] = 0,\ k \geq N \tag{A.6}$$

Thus, $\alpha\mathbf{x} + (1-\alpha)\mathbf{y} \in C_2$ and C_2 is convex. □

Proposition 3. *The set C_3 defined in Equation (3.5) is convex.*

Proof. For any $\mathbf{x}, \mathbf{y} \in C_3$, we have:

$$\begin{aligned}
\sum_{k\neq 0} |\alpha x[k\cdot K] + (1-\alpha)y[k\cdot K]| &\leq \sum_{k\neq 0} |\alpha x[k\cdot K]| + |(1-\alpha)y[k\cdot K]| && \text{(A.7)}\\
&= \alpha \sum_{k\neq 0} |x[k\cdot K]| + (1-\alpha)\sum_{k\neq 0} |y[k\cdot K]| && \text{(A.8)}\\
&\leq \alpha b + (1-\alpha)b && \text{(A.9)}\\
&= b && \text{(A.10)}
\end{aligned}$$

Therefore, $\alpha\mathbf{x} + (1-\alpha)\mathbf{y} \in C_3$ and C_3 is convex. □

Proposition 4. *The set C_4 defined in Equation (3.6) is convex.*

Proof. For any $\mathbf{x}, \mathbf{y} \in C_4$, where $\mathbf{X}, \mathbf{Y}$ are the Fourier transforms of $\mathbf{x}, \mathbf{y}$, respectively, we have:

$$X(\omega), Y(\omega) \in \mathbf{R}, \forall\omega \in \mathbf{R} \Rightarrow \alpha X(\omega) + (1-\alpha)Y(\omega) \in \mathbf{R}, \forall\omega \in \mathbf{R} \tag{A.11}$$

Due to the linearity of the Fourier transform, we have:

$$\alpha\mathbf{x} + (1-\alpha)\mathbf{y} \in C_4 \tag{A.12}$$

Hence, C_4 is convex. □

Proposition 5. *The set C_5 defined in Equation (3.7) is convex.*

Proof. $\forall\, \mathbf{x}, \mathbf{y} \in C_5$, we have the following relations:

$$\alpha x[0] + (1-\alpha)y[0] = \alpha + (1-\alpha) \tag{A.13}$$

and

$$\begin{aligned} |\alpha x[k] + (1-\alpha)y[k]| &\leq |\alpha x[k]| + (1-\alpha)\,|\alpha y[k]| && \text{(A.14)} \\ &\leq \alpha + (1-\alpha) && \text{(A.15)} \\ &= 1 && \text{(A.16)} \end{aligned}$$

Therefore, $\alpha\mathbf{x} + (1-\alpha)\mathbf{y} \in C_5$ and C_5 is convex. □

A.2 Orthogonal Projections

In this section of the appendix, we investigate the conditions for defining orthogonal projection operators given in Equations (3.8),(3.10),(3.12), and (3.13) onto the sets given in Equations (3.3),(3.4),(3.6), and (3.7), respectively.

Proposition 6. *The projection operator defined in Equation (3.8) is orthogonal.*

Proof. Let us define the norm squared error for the projection $S_p(\omega)$ of $S(\omega)$ onto the set C_1 in Equation (3.3):

$$\begin{aligned} \|\mathbf{S_d} - \mathbf{S}\|^2 &= \int |S_d(\omega) - S(\omega)|^2\, d\omega && \text{(A.17)} \\ &= \int\limits_{|S(\omega)|>D(\omega)} |S_d(\omega) - S(\omega)|^2\, d\omega + \int\limits_{|S(\omega)|\leq D(\omega)} |S_d(\omega) - S(\omega)|^2\, d\omega && \text{(A.18)} \\ &\geq \int\limits_{|S(\omega)|>D(\omega)} |D(\omega) - S(\omega)|^2\, d\omega + \int\limits_{|S(\omega)|\leq D(\omega)} |S_d(\omega) - S(\omega)|^2\, d\omega && \text{(A.19)} \\ &\geq \int\limits_{|S(\omega)|>D(\omega)} |D(\omega) - S(\omega)|^2\, d\omega && \text{(A.20)} \end{aligned}$$

with equality if and only if

$$S_p(\omega) = \begin{cases} S(\omega), & |S(\omega)| \leq D(\omega) \\ D(\omega) \cdot e^{j\Phi(\omega)}, & \text{otherwise} \end{cases} \tag{A.21}$$

where $\Phi(\omega)$ is the phase of $S(\omega)$. Therefore, the projection operator in Equation (3.8) is orthogonal. □

Proposition 7. *The projection operator defined in Equation (3.10) is orthogonal.*

Proof. Let us define the norm squared error for the projection $r_p[k]$ of $r[k]$ onto the set C_2 in Equation (3.4):

$$\begin{aligned} \|\mathbf{r_p} - \mathbf{r}\|^2 &= \sum_k |r_p[k] - r[k]|^2 && \text{(A.22)} \\ &= \sum_{k \leq N} |r_p[k] - r[k]|^2 + \sum_{k > N} |r_p[k] - r[k]|^2 && \text{(A.23)} \\ &= \sum_{k \leq N} |r_p[k] - r[k]|^2 + \sum_{k > N} |r[k]|^2 && \text{(A.24)} \\ &\geq \sum_{k > N} |r[k]|^2 && \text{(A.25)} \end{aligned}$$

where $N = \left\lfloor \frac{T_p}{T_s} \right\rfloor$. The equality is satisfied if and only if $r_p[k] = r[k],\ k \leq N$. Therefore the projection operator given in Equation (3.10) is orthogonal. □

Proposition 8. *The projection operator defined in Equation (3.12) is orthogonal.*

Proof. Let us begin with the norm squared error for the projection $\mathbf{r_p}$ of $\mathbf{r}$ onto the set C_4 in Equation (3.6):

$$\begin{aligned} \|\mathbf{r_p} - \mathbf{r}\|^2 &= \|\mathbf{S_p} - \mathbf{S}\|^2 && \text{(A.26)} \\ &= \int |S_p(\omega) - S(\omega)|^2 d\omega && \text{(A.27)} \\ &= \int \{Re\,[S_p(\omega) - S(\omega)]\}^2 d\omega + \int \{Im\,[S_p(\omega) - S(\omega)]\}^2 d\omega && \text{(A.28)} \\ &= \int \{Re\,[S_p(\omega) - S(\omega)]\}^2 d\omega + \int \{Im\,[S_p(\omega) - S(\omega)]\}^2 d\omega && \text{(A.29)} \\ &\geq \int \{Im\,[S(\omega)]\}^2 d\omega && \text{(A.30)} \end{aligned}$$

where the equality is satisfied if and only if

$$S_p(\omega) = Re\left[S(\omega)\right] \tag{A.31}$$

Therefore the projection operator given in Equation (3.12) is orthogonal. □

Proposition 9. *The projection operator defined in Equation (3.13) is orthogonal.*

Proof. Similarly, let us begin with the norm squared error for the projection $r_p[k]$ of $r[k]$ onto the set C_5 in Equation (3.7):

$$\begin{aligned}
\left\|\mathbf{r_p} - \mathbf{r}\right\|^2 &= \sum_k \left|r_p[k] - r[k]\right|^2 && \text{(A.32)}\\
&= \sum_{|r[k]|\leq 1} \left|r_p[k] - r[k]\right|^2 + \sum_{|r[k]|>1} \left|r_p[k] - r[k]\right|^2 && \text{(A.33)}\\
&= \sum_{|r[k]|>1} \left|r_p[k] - r[k]\right|^2 && \text{(A.34)}\\
&\geq \sum_{k>N} \left|r[k]\right|^2 && \text{(A.35)}
\end{aligned}$$

with equality if and only if

$$r_p[k] = \begin{cases} r[k], & |r[k]| \leq 1 \\ \frac{r[k]}{|r[k]|}, & |r[k]| > 1 \end{cases} \tag{A.36}$$

Therefore, the projection operator defined in Equation (3.13) is orthogonal. □

Bibliography

[1] D. C. Youla and H. Webb, "Image restoration by the method of convex projections," *IEEE Trans. Med. Imaging*, MI-1(2):81-94, 1982.

[2] H. Stark. *Image recovery–theory and application* (Orlando, Academic Press, 1987.)

[3] P. L. Combettes, "The foundations of set theoretic estimation," *Proceedings of the IEEE*, vol. 81, no. 2, pp. 182-208, 1993.

[4] M. I. Sezan and H. Stark, "Image restoration by the method of Convex Projections, Part-2: Applications and Numerical Results," *IEEE Trans. Med. Imaging*, vol. MI-1, no.2, pp.95-101, Oct. 1982.

[5] M. I. Sezan and H. Stark. Image restoration by the method of Convex Projections, Part-2: Applications and Numerical Results. *IEEE Trans. on Medical Imaging*, vol. MI-1, no.2, pp.95-101, Oct. 1982.

[6] M. I. Sezan and A. M. Tekalp. Adaptive Image Restoration with artifact suppression using the theory of convex projections. *IEEE Trans. Acoust., Speech, and Signal Proc.,* vol. 38, pp. 181-185, 1990.

[7] H. J. Trussell and M. R. Civanlar, "The Feasible solution in signal restoration," *IEEE Trans. Acoust., Speech, and Signal Proc.,* vol. 32, pp. 201-212, 1984.

[8] A. E. Cetin and R. Ansari, "A convolution based framework for signal recovery," *Journal of Optical Society of America-A*, pp. 1193-1200, vol.5, Aug. 1988.

[9] A. E. Cetin and R. Ansari, "Signal recovery from wavelet transform maxima," *IEEE Trans. Acoust., Speech, and Signal Proc.,* vol. 42, pp. 194-196, Jan. 1994.

[10] A. E. Cetin, O. N. Gerek, and Y. Yardimci, "Equiripple FIR filter design by the FFT algorithm,", *IEEE Signal Processing Magazine*, vol. 14, pp. 60-64, Mar. 1997.

[11] H. M. Ozaktas, Z. Zalevsky, and M. A. Kutay, *The Fractional Fourier Transform with Applications in Optics and Signal Processing* (Wiley, New York, 2001).

[12] H. M. Ozaktas, B. Barshan, D. Mendlovic, and L. Onural. Convolution, filtering, and multiplexing in fractional Fourier domains and their relation to chirp and wavelet transforms. *J Opt Soc Am A*, 11:547–559, 1994.

[13] L. B. Almeida. The fractional Fourier transform and time-frequency representations. *IEEE Trans Signal Processing*, 42:3084–3091, 1994.

[14] D. Mendlovic and H. M. Ozaktas. Fractional Fourier transforms and their optical implementation: I. *Journal of the Optical Society of America A*, 10:1875–1881, 1993.

[15] H. M. Ozaktas and D. Mendlovic. Fractional Fourier transforms and their optical implementation: II. *Journal of the Optical Society of America A*, 10:2522–2531, 1993.

[16] H. M. Ozaktas and D. Mendlovic. Fourier transforms of fractional order and their optical interpretation. *Optics Communications*, 101:163–169, 1993.

[17] M. A. Kutay, H. M. Ozaktas, O. Arıkan, and L. Onural. Optimal filtering in fractional Fourier domains. *IEEE Trans Signal Processing*, 45:1129–1143, 1997.

[18] G. Cariolaro, T. Erseghe, P. Kraniauskas, and N. Laurenti. A unified framework for the fractional Fourier transform. *IEEE Trans Signal Processing*, 46:3206–3219, 1998.

[19] D. Mendlovic, Z. Zalevsky, and H. M. Ozaktas. Applications of the fractional Fourier transform to optical pattern recognition. In F. T. S. Yu and S. Jutamulia, editors, *Optical Pattern Recognition*, pages 89–125 (chapter 4). Cambridge University Press, Cambridge, 1998.

[20] M. F. Erden, M. A. Kutay, and H. M. Ozaktas. Repeated filtering in consecutive fractional Fourier domains and its application to signal restoration. *IEEE Trans Signal Processing*, 47:1458–1462, 1999.

[21] G. Cariolaro, T. Erseghe, P. Kraniauskas, and N. Laurenti. Multiplicity of fractional Fourier transforms and their relationships. *IEEE Trans Signal Processing*, 48:227–241, 2000.

[22] M. A. Kutay, H. Özaktaş, H. M. Ozaktas, and O. Arıkan. The fractional Fourier domain decomposition. *Signal Processing*, 77:105–109, 1999.

[23] İ. Ş. Yetik, M. A. Kutay, H. Özaktaş, and H. M. Ozaktas. Continuous and discrete fractional Fourier domain decomposition. In *Proc 2000 IEEE Int Conf Acoust, Speech, and Signal Process*, pages I:93–96. IEEE, Piscataway, New Jersey, 2000.

[24] M. A. Kutay, and H. M. Ozaktas. Optimal image restoration with the fractional Fourier transform. *J Opt Soc Am A*, 15:825–833, 1998.

[25] B. Barshan and B. Ayrulu. Fractional Fourier transform preprocessing for neural networks and its application to object recognition. *Neural Networks* 15:131–140, 2002.

[26] S.-C. Pei, M.-H. Yeh, and C.-C. Tseng. Discrete fractional Fourier transform based on orthogonal projections. *IEEE Trans Signal Processing*, 47:1335–1348, 1999.

[27] H. M. Ozaktas, O. Arikan, M. A. Kutay, and G. Bozdağı. Digital computation of the fractional Fourier transform. *IEEE Trans Signal Processing*, 44:2141–2150, 1996.

[28] M. J. Bastiaans and A. J. van Leest. From the rectangular to the quincunx Gabor lattice via fractional Fourier transformation. *IEEE Signal Processing Lett*, 5:203–205, 1998.

[29] X.-G. Xia. On bandlimited signals with fractional Fourier transform. *IEEE Signal Processing Lett*, 3:72–74, 1996.

[30] A. I. Zayed. A convolution and product theorem for the fractional Fourier transform. *IEEE Signal Processing Lett*, 5:101–103, 1998.

[31] O. Akay and G. F. Boudreaux-Bartels. Fractional convolution and correlation via operator methods and an application to detection of linear FM signals. *IEEE Trans Signal Processing*, 49:979–993, 2001.

[32] T. Alieva and M. J. Bastiaans. On fractional Fourier transform moments. *IEEE Signal Processing Lett*, 7:320–323, 2000.

[33] T. Erseghe, P. Kraniauskas, and G. Cariolaro. Unified fractional Fourier transform and sampling theorem. *IEEE Trans Signal Processing*, 47:3419–3423, 1999.

[34] S. C. Pei and M. H. Yeh. The discrete fractional cosine and sine transforms. *IEEE Trans Signal Processing*, 49:1198–1207, 2001.

[35] İ. Ş. Yetik, H. M. Ozaktas, B. Barshan, and L. Onural. Perspective projections in the space-frequency plane and fractional Fourier transforms. *Journal of the Optical Society of America A*, 17:2382–2390, 2000.

[36] S. T. Liu, L. Yu, and B. H. Zhu. Optical image encryption by cascaded fractional Fourier transforms with random phase filtering. *Opt Commun*, 187:57–63, 2001.

[37] J. T. Sheridan and R. Patten. Holographic interferometry and the fractional Fourier transformation. *Opt Lett*, 25:448–450, 2000.

[38] H. M. Ozaktas and O. Aytür. Fractional Fourier domains. *Signal Processing*, 46:119–124, 1995.

[39] L. Barker, Ç. Candan, T. Hakioğlu, M. A. Kutay, and H. M. Ozaktas. The discrete harmonic oscillator, Harper's equation, and the discrete fractional Fourier transform. *Journal of Physics A*, 33:2209–2222, 2000.

[40] H. M. Ozaktas, D. Mendlovic. Fractional Fourier optics. *J Opt Soc Am A*, 12:743–751, 1995.

[41] H. M. Ozaktas and David Mendlovic. Fractional Fourier transform as a tool for analyzing beam propagation and spherical mirror resonators. *Optics Letters*, 19:1678–1680, 1994.

[42] M. F. Erden, H. M. Ozaktas, and D. Mendlovic. Synthesis of mutual intensity distributions using the fractional Fourier transform. *Opt Commun*, 125:288-301, 1996.

[43] J. R. Fienup, "Phase retrieval algorithms: a comparison," *J. Opt. Soc. Am. A*, vol. 21, no. 15: 2758:2769, 1982.

[44] J. G. Proakis, *Digital Communications*, McGraw Hill, New York, 2001.

[45] A. V. Oppenheim, and R. W. Schafer, *Discrete-Time Signal Processing*, Prentice Hall, Englewood Cliffs, New Jersey, 1989.

[46] A. N. Nobakht and M. R. Civanlar, "Optimal pulse shape design for digital communication systems by using projections onto convex sets," *IEEE Trans. Communications*, vol. 43, no.12: 2874-2877, 1995.

[47] Ç. Candan, M. A. Kutay, and H. M. Ozaktas. The discrete fractional Fourier transform. *IEEE Trans Signal Processing*, 48:1329–1337, 2000.

[48] P. L. Combettes. The Convex Feasibility Problem in Image Recovery. *Advances in Imaging and Electron Physics*, vol. 95, pp. 155-270, Academic Press, New York, 1996.

[49] A. E. Cetin, H. Özaktaş, and H. M. Ozaktas. Resolution enhancement of low resolution wavefields with POCS algorithm. *Electronics Letters*, 39:1808–1810, 2003.

[50] Z. Zalevsky and D. Mendlovic. Fractional Wiener filter. *Applied Optics*, Vol. 35 Issue 20, p. 3930, July 1996.

[51] B. Barshan, M. A. Kutay, and H. M. Ozaktas. Optimal filtering with linear canonical transformations. *Optics Communications*, 135:32–36, 1997.